Bulletin of the Chemical Society of Japan

Strategically Designed Zeolitic Imidazolate Frameworks for Controlling the Degree of Graphitization

Sang A Han, Jaewoo Lee, Kyubin Shim, Jianjian Lin, Mohammed Shahabuddin, Jong-Won Lee, Sang-Woo Kim, Min-Sik Park, and Jung Ho Kim*

Advance Publication on the web August 2, 2018

doi:10.1246/bcsj.20180174

Strategically Designed Zeolitic Imidazolate Frameworks for Controlling the Degree of Graphitization

Sang A Han,[1,5] Jaewoo Lee,[1] Kyubin Shim,[1] Jianjian Lin,[2] Mohammed Shahabuddin,[3] Jong-Won Lee,[4] Sang-Woo Kim,[5] Min-Sik Park,[6] Jung Ho Kim*[1,6]

[1]Institute for Superconducting and Electronic Materials (ISEM), Australian Institute for Innovative Materials (AIIM), University of Wollongong, North Wollongong, NSW 2500, Australia

[2]College of Chemistry and Molecular Engineering Qingdao University of Science and Technology, Qingdao 266042, China

[3]Department of Physics and Astronomy, College of Science, King Saud University, P.O. Box 2455, Riyadh 11451, Saudi Arabia

[4]Department of Materials Science and Engineering, Chosun University, 309 Pilmun-daero, Dong-gu, Gwangju 61452, Republic of Korea

[5]School of Advanced Materials Science & Engineering, Sungkyunkwan University (SKKU), Suwon, 440-746, Republic of Korea

[6]Department of Advanced Materials Engineering for Information and Electronics, Kyung Hee University, 1732 Deogyeong-daero, Giheung-gu, Yongin-si, Gyeonggi-do, 17104, Republic of Korea

E-mail: <jhk@uow.edu.au>

Prof. Jung Ho Kim is currently tenured Professor at the Institute for Superconducting and Electronic Materials (ISEM), Australian Institute for Innovative Materials (AIIM), University of Wollongong, Australia. He received his Bachelor's (1998), Master's (2000), and Ph.D (2005) degrees from Sungkyunkwan University, Korea. He is currently acting as an editorial board member for Scientific Reports (Nature Publishing Group) and and associate editor for Science and Technology of Advanced Materials. His major research is the rational design of materials for energy storage and harvesting applications.

Abstract

The zeolitic imidazolate frameworks (ZIFs) ZIF-8 and ZIF-67 are well-known as belonging to the series of metal-organic frameworks. Using different types of metal ions in them, such as Zn^{2+} and Co^{2+} simultaneously, brings both advantages and disadvantages with respect to the carbonization process. For tailoring their properties, we suggest that the best approach involves control of the bimetallic ZIF-derived carbon nanoarchitecture, which is hybridized through the synergistic effects of each metal ion. In this study, the bimetallic ZIFs were designed by controlling the molar ratio of zinc (Zn^{2+}) and cobalt (Co^{2+}) ions, and the carbon nanoarchitecture was subsequently formed by a facile heat treatment and acid leaching. We demonstrate this approach to achieve tailored ZIF derived carbon nanoarchitectures with different pore sizes, surface areas, and degree of graphitization. These pave the way to finding the optimal carbon nanoarchitecture for specific applications such as Li-O_2 air cell.

Keywords: zeolitic imidazolate frameworks, bimetallic metal-organic frameworks, graphitization

1. Introduction

Metal-organic frameworks (MOFs) (or porous coordination polymers (PCPs)) are well known to consist of metal ions and organic molecule (called the 'linker') to build a permanent porous structure with different functionalities.[1-11] Without any soft or hard template, the MOFs possess a unique feature, forming pore structures or certain voids because the repeated organic linker and secondary building blocks act as the template.[12,13] Two important ways to tune MOF-derived nanoarchitectures are by the linker geometries and selection of metal ions.[14] Importantly, the MOFs can easily be converted to various metal oxides or new carbonaceous materials through different calcination temperatures /atmospheres and chemical treatment. Thus, these structures are highly attractive for a variety of industrial applications, such as energy storage/harvesting devices, sensors, H_2/CO_2 capture, drug delivery, and catalysts.[15-26]

The synthesis of the MOFs was originally developed based on zeolite chemistry. Kitagawa[27] and Yaghi[28,29] strategically designed and developed various inorganic-organic structures. Since then, approximately 20,000 MOFs have been reported.[30] In particular, MOF-5[31] and HKUST-1[32] are representative of the first step for various applications. Zeolitic imidazolate frameworks (ZIFs) are one subclass in the MOF family.[33,34] The thermal, chemical, and mechanical satability of the MOFs still needs to be further enhanced to reach commercial quality. However, ZIFs follow the crystalline structure of natural zeolite, which is suitable for thermal stability in a wide temperature range, thus thermal expansion and chemical stability are much higher than for other MOFs. To overcome these drawbacks, ZIFs or covalent organic frameworks (COFs) are highly expected to open up many possibilities. Representative ZIF-8 and ZIF-67 MOFs, which composed of metal ions of Zn^{2+} and Co^{2+}, respectively, strongly coordinated by 2-methylimidazole (2-MIM) organic linkers, are formed as rhombic dodecahedra with a large cavity (11.6 Å).[35,36] The interior cavities directly introduce robust pores, but form different features through the calcination process. More significantly, Yamauchi [37] and Park [38] suggested a straightforward way to make hierarchically porous carbons without a secondary carbon precursor. These have gained great attention because they allow a direct carbonaceous approach with the ZIF series.

In this study, combining the different metal ions Zn^{2+} and Co^{2+} is expected to yield different properties, such as high surface area, a good degree of graphitization, electrical conductivity, high nitrogen content, and chemical stability. For various applications, we have carefully evaluated our ZIF derived carbons with different molar ratios of Zn^{2+} and Co^{2+}, and then systematically compared them with directly carbonized ZIF-8 and ZIF-67 structures. The Li-O_2 cell was fabricated and its discharge-charge Galvanostatic measurement was carried out in order to investigate the possibility of application to an air cell as an energy storage device.

2. Experimental

Preparation of ZIF-8 Crystals. Zinc nitrate hexahydrate ($Zn(NO_3)_2{\cdot}6H_2O$, 891 mg, 3 mmol) was dissolved in methanol (CH_3OH, 30 mL). 2-methylimidazole ($CH_3C_3H_2N_2H$, 984 mg, 12 mmol) was separately dissolved in methanol (10 mL). Subsequently, the metal precursor solution was poured into the solution in which 2-methylimidazole was dissolved and stirred. The resulting solution was kept at 100 °C for 12 hours. The product was filtered, thoroughly washed with methanol, and then dried at 80 °C. The ZIF-8 powder was further activated at 120 °C under vacuum for 24 hours.

Preparation of ZIF-67 Crystals. Cobalt nitrate hexahydrate ($Co(NO_3)_2{\cdot}6H_2O$, 873 mg, 3 mmol) was dissolved in methanol (CH_3OH, 30 mL). 2-methylimidazole ($CH_3C_3H_2N_2H$, 984 mg, 12 mmol) was separately dissolved in methanol (CH_3OH, 10 mL). Subsequently, the metal precursor solution was poured into the solution in which 2-methylimidazole was dissolved and stirred. The resulting solution was kept at 100 °C for 12 hours. The product was filtered, thoroughly washed with methanol and then dried at 80 °C. The ZIF-67 powder was further activated at 120 °C under vacuum for 24 hours.

Preparation of Co/Zn ZIF Crystals. The synthesis procedure for the Zn/Co ZIF crystals is similar to the synthesis procedure for other members of the ZIF series. The desired molar ratio of zinc to cobalt ions (Zn^{2+}/ Co^{2+}) was dissolved in methanol (30 ml) using zinc nitrate hexahydrate and cobalt nitrate hexahydrate, and stirred for 1 hour. 2-methylimidazole was dissolved in methanol (10 ml), and the two metal precursor solutions were poured into the as-prepared imidazole solution and stirred until the mixture was homogeneous. The resulting solution was kept at 100 °C for 12 hours. The product was filtered, thoroughly washed with methanol and then dried at 80 °C. The bimetallic Zn/Co ZIF powder was further activated at 120 °C under vacuum for 24 hours.

Preparation of Nanoporous Carbon Materials from bimetallic ZIFs. To obtain the nanoporous ZIF derived carbon material, the activated hybrid ZIF powder was sintered at a heating rate of 2-5 °C·min^{-1} and carbonized at 900 °C for 2 hours under Ar atmosphere, before being cooled down to room temperature. The resulting bimetallic ZIF derived carbon was washed with hydrogen fluoride solution (HF(aq)) and a large amount of water and methanol to remove any remaining metal ions. The product was finally dried at 120 °C for 12 hours.

Characterizations. The morphologies and particle sizes of the ZIF-8, ZIF-67, and bimetallic ZIF derived carbon nanoarchitectures were confirmed using field emission scanning electron microscopy (FESEM, JEOL JSM-7000F). The crystalline structure were investigated using an X-ray diffraction (XRD, Malvern Panalytical, Empyrean) with Cu-Kα radiation (λ = 1.54056 Å). The crystallinity and microstructure were obtained using high resolution transmission electron microscopy (HRTEM, JEOL ARM-200F) with a Cs corrector (CEOS GmbH). The specific surface area and pore volume were characterized by the Brunauer-Emmett-Teller (BET) and

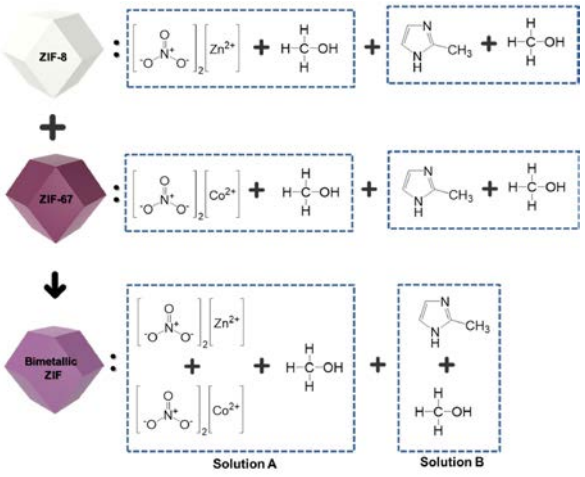

Figure 1. Schematic illustration of the concept of this paper, the synthesis of bimetallic ZIFs by hybridization of ZIF-8 and ZIF-67. Zinc nitrate hexahydrate and cobalt nitrate hexahydrate sources (Solution A) were used as the metal precursor and 2-methylimidazole (Solution B) was used as the organic linker.

Barrett-Joyner-Halenda (BJH) methods using a surface area and porosimetry analyzer (Micromeritics, Tristar II 3020). **Electrochemical Experiments.** A Li-O_2 cell was constructed based on a Swagelok design and composed of a Li metal anodes, an electrolyte (1 M LiTFSI in TEGDME) impregnated into a glass fiber separator and a cathode. The cathode was prepared by casting a mixture of ZIF-8, ZIF-67 and various molar ratio of Co/Zn cryatals, conducting carbon (Super-P) and a binder (Kynar 2801) (80:15:5 in wt.%) in NMP on a Ni mesh current collector, followed by vacuum drying at 70 °C for 24 h. The electrode loading was 2 mg·cm^{-2}. Discharge-charge profiles were measured at a current density of 50 mA·g^{-1} using a Maccor Series 4000. All of the electrochemical experiments were conducted at 30 °C by supplying a high-purity O_2 (99.99%) gas.

3. Results and Discussion

The strategic design of the synthesis for various ZIF derived carbons is simply summarized in **Figure 1**. In order to obtain the bare ZIF-8, ZIF-67, and bimetallic ZIF, different metal precursors and 2-methylimidazole were used along with methanol in an aqueous solution. In addition, the bimetallic ZIFs were obtained by controlling the molar ratio of zinc to cobalt ions (Zn^{2+}/Co^{2+}). Herein, the molar ratios of zinc to cobalt ions were 199:1, 19:1, 9:1, 2:1, 1:2, and 1:4, and denoted as $Zn_{0.995}{\cdot}Co_{0.005}$, $Zn_{0.95}{\cdot}Co_{0.05}$, $Zn_{0.9}{\cdot}Co_{0.1}$, $Zn_{0.67}{\cdot}Co_{0.33}$, $Zn_{0.33}{\cdot}Co_{0.67}$, and $Zn_{0.2}{\cdot}Co_{0.8}$, respectively.

Figure 2 shows FESEM images and their size distribution results for ZIF-8 and ZIF-67 derived carbons as reference, and various bimetallic ZIF derived carbons with different molar ratios of zinc to cobalt ions. From our observations, the morphology of bimetallic ZIFs derived carbons is the same as for the parent structures of bare ZIF-8 and ZIF-67, having a rhombic dodecahedral particle shape. Interestingly, the shape shows some swelling with increasing relative molar ratios of zinc to cobalt ions. This indicates that one role of the zinc ions is to maintain the polyhedral structure in the bimetallic ZIFs derived carbon. It should be noted that the ZIF derived carbon with excess cobalt ions ($Zn_{0.33}{\cdot}Co_{0.67}$) clearly generates rich

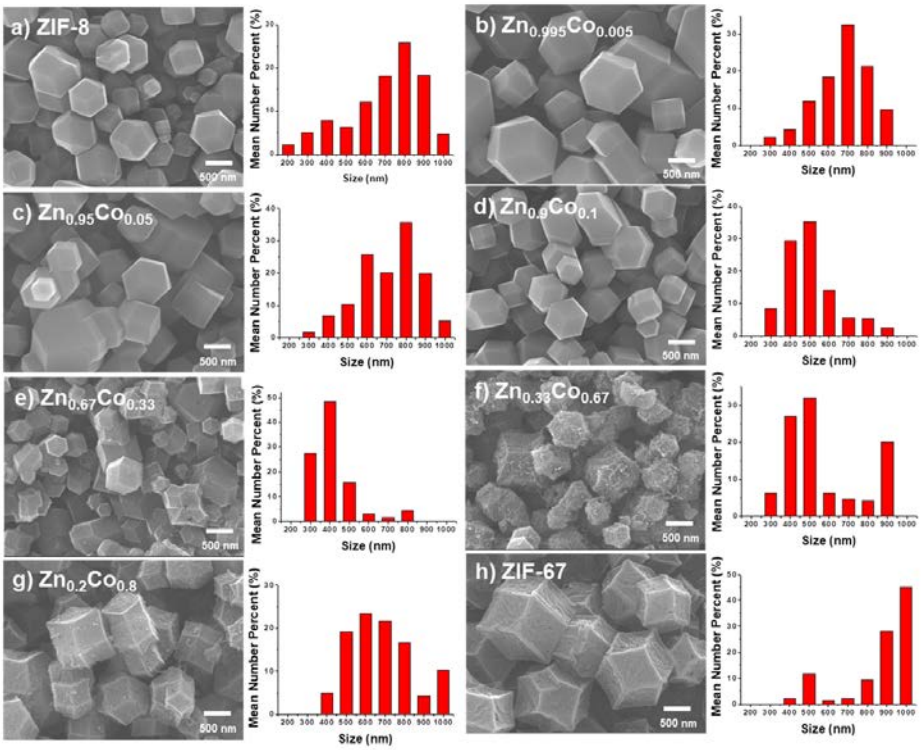

Figure 2. FESEM images and size distribution graphs of ZIF derived carbons: (a) ZIF-8 derived carbon; bimetallic ZIF derived carbons with different molar ratios of zinc to cobalt ions: (b) $Zn_{0.995}$·$Co_{0.009}$, (c) $Zn_{0.95}$·$Co_{0.05}$, (d) $Zn_{0.9}$·$Co_{0.1}$, (e) $Zn_{0.67}$·$Co_{0.33}$, (f) $Zn_{0.33}$·$Co_{0.67}$, and (g) $Zn_{0.2}$·$Co_{0.8:}$ and (h) ZIF-67 derived carbon.

graphitic structure on the surface, as can be seen in **Figure 2f.** This can be attributed to its superior electrical conductivity. We also found that the particle size for all carbons is distributed in the range of 200 nm to 1000 nm, with each carbon having a different average diameter. For example, the average particle size of ZIF-8 or ZIF-67 derived carbon is estimated to be 500 nm and 1000 nm, respectively. In particular, the ZIF-67 derived carbon has a relatively large particle size compared to other ZIF series carbons. This is due to the different kinetic reactions of cobalt and zinc ions in 2-methylimidazole. Even in this work, however, there is no particular tendency in the size distribution according to the molar ratio of zinc to cobalt ions. Only a trend in surface roughness is clearly visible in our results.

XRD analysis was performed to confirm the degree of graphitization for various bimetallic ZIF derived carbons, as can be seen in **Figure 3**. In the case of ZIF-8 derived carbon with only zinc ions, the broad diffraction peaks at 24° and 44° represent the (002) and (101) planes of typical amorphous carbon. It should be noted that the full-width at half maximum of the C (002) peak at about 24° becomes narrow due to the molar ratio of the cobalt ions of 0.33. This indicates that the amorphous carbon gradually becomes graphitic, and its crystallinity also improves. These results indicate that cobalt metal ions can be related to the degree of graphitization. Moreover, as the molar ratio of cobalt to zinc ions increases, Co (111) and (200) peaks clearly appear, which are not seen from ZIF-8 to $Zn_{0.9}$·$Co_{0.1}$. That is to say, trapped cobalt particles are hard to remove by carbonization and the acid leaching process. Zinc ones have relatively low melting and boiling temperatures, however, at around 419 °C and 907 °C, respectively. During the carbonization at 900 °C in this study, most zinc particles can be easily removed.

The crystallinity of as-prepared carbons can also be confirmed from the HRTEM images shown in **Figure 4**. The

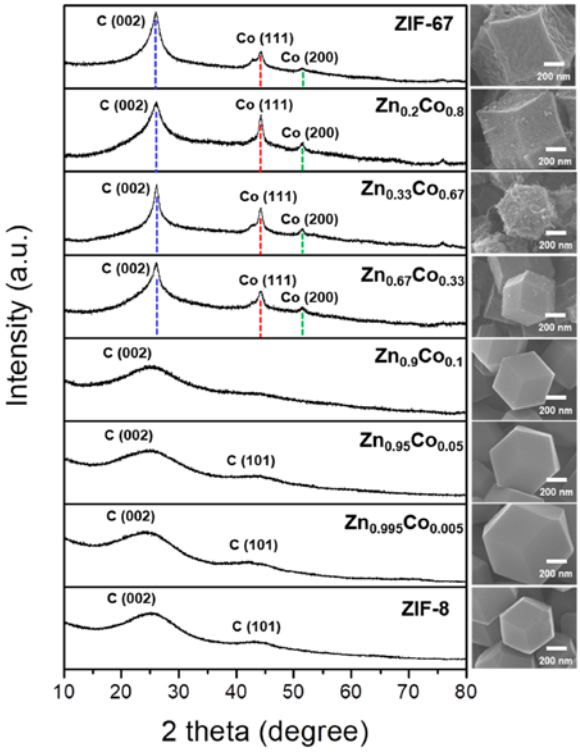

Figure 3. XRD patterns of ZIF-8, ZIF-67 and various bimetallic ZIFs derived carbons with different molar ratios of zinc to cobalt ions. Right column shows representative FESEM images.

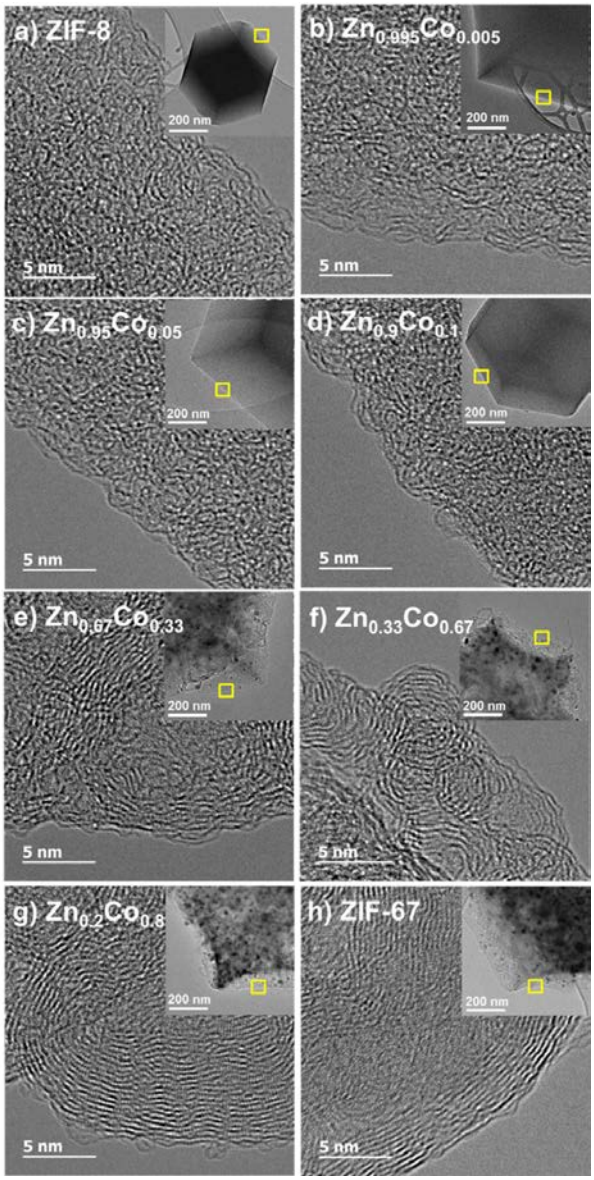

Figure 4. HRTEM images of (a) ZIF-8 derived carbon; (b) bimetallic ZIF derived carbons with different molar ratios of zinc to cobalt ions with $Zn_{0.995}$·$Co_{0.009}$, (c) $Zn_{0.95}$·$Co_{0.05}$, (d) $Zn_{0.9}$·$Co_{0.1}$, (e) $Zn_{0.67}$·$Co_{0.33}$, (f) $Zn_{0.33}$·$Co_{0.67}$, and (g) $Zn_{0.2}$·$Co_{0.8}$: and (h) ZIF-67 derived carbon.

insets show the corresponding low-magnification images of various ZIF derived carbons with different molar ratios of zinc to cobalt ions. From cobalt-ion-free ZIF-8 to $Zn_{0.9}$·$Co_{0.1}$ derived carbon, where the cobalt ions content is less than the zinc one, amorphous carbon is obviously formed, as shown in **Figure 4a–4d**. It can be seen that the crystallinity of the thus-formed ZIF derived carbons is improved as the molar ratio of cobalt ions increases, as shown in **Figure 4e–4h**. These results clearly argued that the bimetallic ZIFs are effectively graphitized in the existence of certain cobalt amount, which indicate the shrinkage of facets and distorted polyhedral structure. Especially in the case of $Zn_{0.33}$·$Co_{0.67}$ derived carbon, it can be confirmed that carbon nanotubes (CNTs) are formed on the surface with very well aligned carbon structure. Very interestingly, the $Zn_{0.67}$·$Co_{0.33}$, $Zn_{0.2}$·$Co_{0.8}$, and ZIF-67 derived carbons also had particles with graphite carbon shells (see

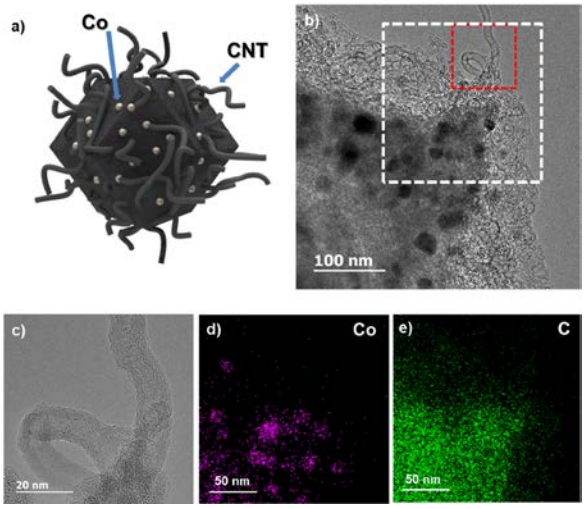

Figure 5. (a) Schematic illustration of bimetallic ZIF derived carbon with zinc to cobalt molar ratio of $Zn_{0.33}$·$Co_{0.67}$. (b) TEM image of $Zn_{0.33}$·$Co_{0.67}$ bimetallic ZIF derived carbon. (c) High resolution TEM image of CNT structure in the area enclosed by the red dashed line in (b). Element mapping images of (d) cobalt and (e) carbon in the area enclosed by the white dashed line in (b).

Figure 3), but no CNTs were observed. This suggests that there is an optimum molar ratio of zinc to cobalt ions in bimetallic ZIFs to promote the growth of CNTs on the surface. This will be discussed in more detail in **Figure 5**. All HRTEM observations show once again the importance of the cobalt content in the formation of bimetallic ZIF derived carbon, as discussed in connection with the XRD results (**Figure 3**).

The CNT structure that appears in the $Zn_{0.33}$·$Co_{0.67}$ derived carbon is shown in **Figure 5** and should be discussed in more detail. **Figure 5a** is a schematic illustration of the CNT structure formed on the $Zn_{0.33}$·$Co_{0.67}$ derived hierarchical carbon structure. This can be further confirmed by HRTEM images (**Figure 5b and 5c**). From the images, the formation of CNTs basically improves the electrical conductivity and might provide some voids/space between $Zn_{0.33}$·$Co_{0.67}$-derived carbons. It has been reported that CNTs are formed due to the cobalt nanoparticles acting as a catalyst on the surface. [16] The energy dispersive X-ray spectroscopy (EDX) of the white square in **Figure 5b** shows that most of the $Zn_{0.33}$·$Co_{0.67}$ derived carbon is well carbonized, but a small fraction of cobalt particles still exist. In contrast, zinc nanoparticles (not shown here) have almost disappeared due to their low vaporization temperature. This confirms that cobalt element plays a key role in the existing of CNTs.

The porosity of bimetallic ZIF derived carbons with different molar ratios of zinc to cobalt ions was investigated using nitrogen adsorption - desorption isotherms. In **Figure 6a**, sharp nitrogen uptake at $P/P_0 < 0.1$ can be related to the strong nitrogen adsorption in micropores. We clearly observed that the ZIF-8, $Zn_{0.995}$·$Co_{0.005}$, $Zn_{0.95}$·$Co_{0.05}$, and $Zn_{0.9}$·$Co_{0.1}$ derived carbon samples show much sharper nitrogen uptake compared to the $Zn_{0.67}$·$Co_{0.33}$, $Zn_{0.33}$·$Co_{0.67}$, $Zn_{0.2}$·$Co_{0.8}$, and ZIF-67 derived carbon samples. As a result, zinc ions as an additive can generate a majority population of micropores, rather than mesopores. All samples show gradual nitrogen uptake in the intermediate relative pressure region between 0.3 and 0.9,

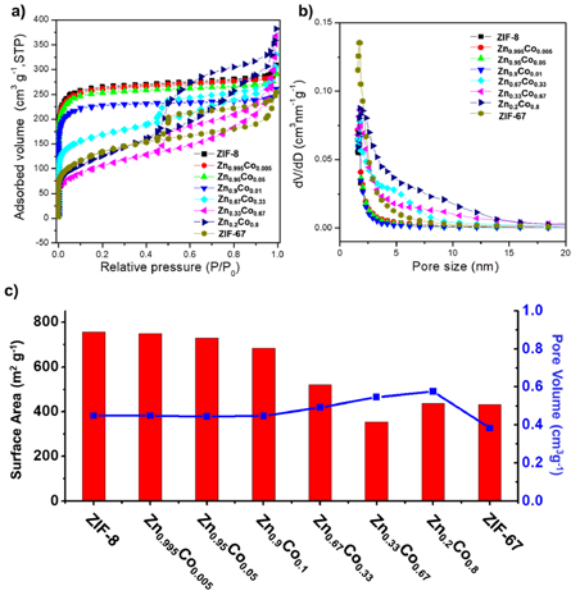

Figure 6. (a) N_2 adsorption-desorption isotherms results, (b) pore size distribution results, and (c) surface area and pore volume graph of ZIF-8, bimetallic ZIF derived carbons, which have zinc to cobalt molar ratios of $Zn_{0.995}$·$Co_{0.009}$, $Zn_{0.95}$·$Co_{0.05}$, $Zn_{0.9}$·$Co_{0.1}$, $Zn_{0.67}$·$Co_{0.33}$, $Zn_{0.33}$·$Co_{0.67}$, and $Zn_{0.2}$·$Co_{0.8}$, and ZIF-67 derived carbon.

indicating the presence of mesopores with a broad size distribution. Most interestingly, the $Zn_{0.67}$·$Co_{0.33}$, $Zn_{0.33}$·$Co_{0.67}$, $Zn_{0.2}$·$Co_{0.8}$, and ZIF-67 derived samples show obvious hysteresis loops. This is mainly due to the increase in widespread mesopores.

The pore size distributions show that the majority population of micropores gradually changes to mesopores with increasing cobalt ions in the bimetallic ZIF derived carbon, as shown in **Figure 6b**. From ZIF-8 derived carbon to the bimetallic ZIF one derived from $Zn_{0.9}$·$Co_{0.1}$, most pores are less than 2 nm in size. We argue that the surface area of each sample is strongly related to the molar ratio of cobalt to zinc in bimetallic ZIFs. **Figure 6c** also shows the pore volume and specific surface area of ZIF-8, ZIF-67, and bimetallic ZIF derived carbons with various molar ratio of zinc to cobalt ions. The specific surface areas decrease from ZIF-8 (756 $m^2 \cdot g^{-1}$), to $Zn_{0.995}$·$Co_{0.005}$ (748 $m^2 \cdot g^{-1}$), $Zn_{0.95}$·$Co_{0.05}$ (729 $m^2 \cdot g^{-1}$), $Zn_{0.9}$·$Co_{0.1}$ (683 $m^2 \cdot g^{-1}$), $Zn_{0.67}$·$Co_{0.33}$ (520 $m^2 \cdot g^{-1}$), and $Zn_{0.33}$·$Co_{0.67}$ (354 $m^2 \cdot g^{-1}$). It then slightly increases in $Zn_{0.2}$·$Co_{0.8}$ (436 $m^2 \cdot g^{-1}$) and ZIF-67 (432 $m^2 \cdot g^{-1}$). In contrast, pore volume tends to decrease as the molar ratio of zinc ions increases. In other words, on decreasing the molar ratio of zinc ions to cobalt ions, the pore size of the thus-formed carbon structure increases, thereby reducing the surface area and increasing the pore volume. This suggests that carbon structures with the desired characteristics such as optimized surface area and pore size can be formed by adjusting the molar ratio of zinc to cobalt ions in the synthesis of Zn/Co bimetallic ZIFs.

Figure 7 shows the Galvanostatic discharge-charge results of our ZIF derived carbon samples. **Figure 7a** is a schematic illustration of the discharge-charge mechanism of the ZIF derived carbon based Li-O_2 air-cell. Capacitance is gradually decreased in the order of ZIF-8, $Zn_{0.995}$·$Co_{0.005}$, $Zn_{0.95}$·$Co_{0.05}$, and $Zn_{0.9}$·$Co_{0.1}$, because the surface area and porosity are reduced as shown in **Figure 7b-7e**. $Zn_{0.67}$·$Co_{0.33}$, $Zn_{0.33}$·$Co_{0.67}$, $Zn_{0.2}$·$Co_{0.8}$ and ZIF-67 show relatively higher capacity compared to the others, which can be explained by the presence of mesopores as shown in **Figure 7f–7i** It is interesting to note that $Zn_{0.33}$·$Co_{0.67}$ in **Figure 7g** shows the highest capacity among the samples tested, which may be

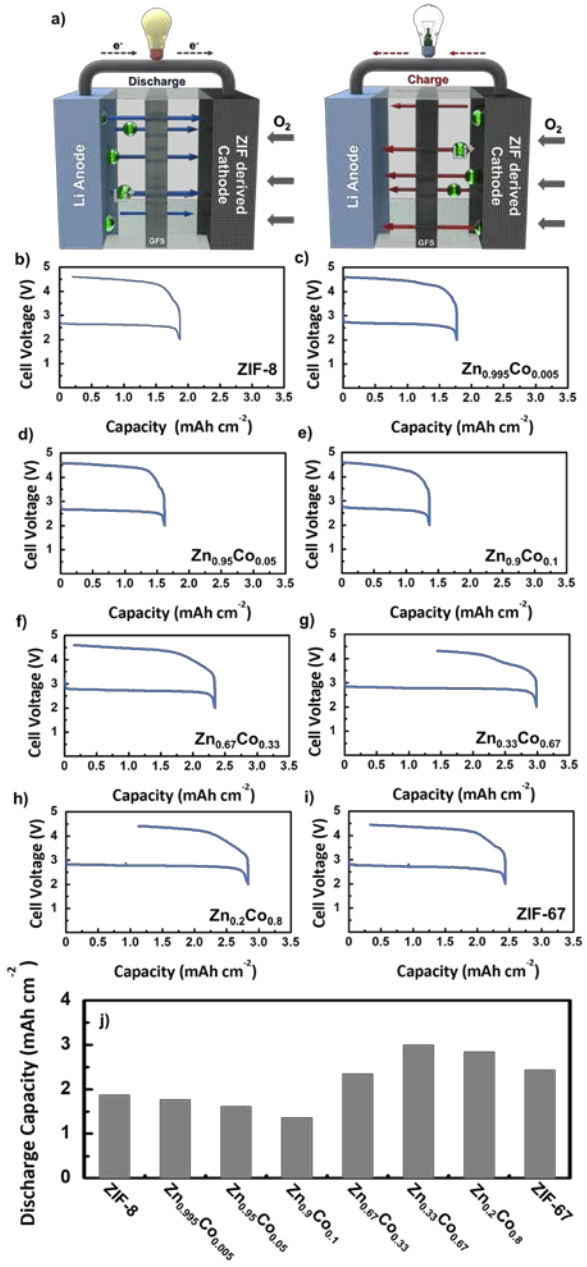

Figure 7. (a) Schematic illustration of the discharge-charge mechanism of the ZIF derived carbon based Li-O_2 air-cell. Galvanostatic discharge-charge results of (b) ZIF-8 derived carbon; (c) bimetallic ZIF derived carbons with different molar ratios of zinc to cobalt ions with $Zn_{0.995}$·$Co_{0.009}$, (d) $Zn_{0.95}$·$Co_{0.05}$, (e) $Zn_{0.9}$·$Co_{0.1}$, (f) $Zn_{0.67}$·$Co_{0.33}$, (g) $Zn_{0.33}$·$Co_{0.67}$, and (h) $Zn_{0.2}$·$Co_{0.8}$: and (i) ZIF-67 derived carbon. (j) Summary of the all results.

explained in terms of the synergistic role of mesopores and Co particles to catalyze CNT growth. This is supported by the previous results that CNTs grow on the surface due to the role of Co particles in the $Zn_{0.33}$·$Co_{0.67}$ case and due to improve of the conductivity.

4. Conclusion

Strategically designed bimetallic ZIF derived carbons with different molar ratios of cobalt to zinc ions were synthesized to clearly understand their material properties for various applications. In this system, the role of zinc ions is to create micropores and maintain a rhombic dodecahedral particle shape without any morphological damage. The role of cobalt ions is to form cobalt nanoparticles, which act as catalytic sites to activate CNTs growth in the carbon. This can improve the electrical conductivity and the amount of space between ZIF derived carbons. By controlling other factors for bimetallic ZIFs, we expect that this type of functional carbon will be highly attractive for Li-O_2 air cell applications.

Acknowledgement

This research was supported by the Korea Institute of Energy Technology Evaluation and Planning (KETEP), and the Ministry of Trade, Industry & Energy (MOTIE) of the Republic of Korea (No. 20152020104870). We also acknowledge the international scientific partnership at King Saud University for funding this research work through ISPP #0095.

References

1. K. S. Park, Z. Ni, A. P. Côté, J. Y. Choi, R. Huang, F. J. Uribe-Romo, H. K. Chae, M. O'Keeffe, O. M. Yaghi, *Proc. Natl. Acad. Sci. USA* **2006**, 103, 10186.
2. R. R. Salunkhe, J. Tang, N. Kobayashi, J. Kim, Y. Ide, S. Tominaka, J. H. Kim, Y. Yamauchi, *Chem. Sci*. **2016**, 7, 5704.
3. W. Chaikittisilp, M. Hu, H. Wang, H. S. Huang, T. Fujita,K. C. Wu, L. C. Chen, Y. Yamauchi, K. Ariga, *Chem. Commun*. **2012**, 48, 7259.
4. H. Wang, Q.-L. Zhu, R. Zou, Q. Xu, Chem 2017, 2, 52
5. V. Malgras, Q. Ji, Y. Kamachi, T. Mori, F. –K. Shieh, K. C. –W. Wu, K. Ariga, Y. Yamauchi, *Bull. Chem. Soc. Jpn.* **2015**, 88, 1171.
6. T. Yamada, M. Sadakiyo, A. Shigematsu, H. Kitagawa, *Bull. Chem. Soc. Jpn.* **2016**, 89, 1.
7. Y. Guo, J. Tang, R. R. Salunkhe, Z. A. Alothman, Md. S. A. Hossain, V. Malgras, Y. Yamauchi, *Bull. Chem. Soc. Jpn*. **2017**, 90, 939.
8. M. Ishidoshiro, H. Imoto, K. Naka, *Bull. Chem. Soc. Jpn.* **2016**, 89, 1057
9. F. –K. Shieh, S. –C. Wang, C. –I. Yen, C. –C. Wu, S. Dutta, L. –Y. Chou, J. V. Morabito, P. Hu, M. –H. Hsu, K. C. –W. Wu, C. –K. Tsung, *J. Am. Chem. Soc*. **2015**, 137, 4276.
10. F. –S. Liao, W. –S. Lo, Y. –S. Hsu, C. –C. Wu, S. –C. Wang, F. –K. Shieh, J. V. Morabito, L. –Y. Chou, K. C. –W. Wu, C. –K. Tsung, *J. Am. Chem. Soc*. **2017**, 139, 6530.
11. Y. V. Kaneti, J. Tang, R. R. Salunkhe, X. Jiang, A. Yu, K. C. –W. Wu, Y. Yamauchi, *Adv. Mater.* **2017**, 29, 1604898.
12. R. R. Salunkhe, Y. V. Kaneti, J. Kim, J. H. Kim, Y. Yamauchi, *Acc. Chem. Res*. **2016**, 49, 2796.
13. S. Dang, Q.–L. Zhu, Q. Xu, *Nature Reviews Materials* **2017**, 3, 17075
14. W. Lu, Z. Wei, Z. –Y. Gu, T. –F. Liu, J. Park, J. Park, J. Tian, M. Zhang, Q. Zhang, T. Gentle III, M. Bosch, H. –C. Zhou, *Chem. Soc. Rev.*, **2014**, 43, 5561.
15. A. V. Vinogradov, H. Z. Hertling, E. H. Hawkins, A. V. Agafonov, G. A. Seisenbaeva, V. G. Kessler, V. V. Vinogradov, *Chem. Commun*. **2014**, 50, 10210
16. S. Goswami, L. Ma, A. B. F. Martinson, M. R. Wasielewski, O. K. Farha, J. T. Hupp, *ACS Appl. Mater. Interfaces* **2016**, 8, 30863
17. Y.-J. Li, J.-M. Fan, M.-S. Zheng, Q.-F. Dong, *Energy Environ. Sci*. **2016**, 9, 1998
18. B. Yang, H. Liu, R. Lv, H. Li, X. Fu, J. Su, X. Liu, W. Gu, *Bull. Chem. Soc. Jpn.*, **2018**, 91, 548.
19. J. Kim, C. Young, J. Lee, M.-S. Park, M. Shahabuddin, Y. Yamauchi, J. H. Kim, *Chem. Commun*. **2016**, 52, 13016
20. M. Ding, W. Shi, L. Guo, Z. Y. Leong, A. Baji, H. Y. Yang, *J. Mater. Chem. A* **2017**, 5, 6113
21. Y. Wu, Z. Zhang, S. Bandow, K. Awaga, *Bull. Chem. Soc. Jpn*. **2017**, 90, 1382.
22. K. Inoue, *Bull. Chem. Soc. Jpn*. **2016**, 89, 1416.
23. K. C. –W. Wu, Y. Yamauchi, *J. Mater. Chem.* **2012**, 22, 1251.
24. H. Kataoka, T. Nakanishi, S. Omagari, Y. Takabatake, Y. Kitagawa, Y. Hasegawa, *Bull. Chem. Soc. Jpn.* **2016**, 89, 103.
25. Y. Tobe, K. Tahara, S. D. Feyter, *Bull. Chem. Soc. Jpn.* **2016**, 89, 1277.
26. T. Wang, Z. Kou, S. Mu, J. Liu, D. He, I. S. Amiinu, W. Meng, K. Zhou, Z. Luo, S. Chaemchuen, F. Verpoort, *Adv. Funct. Mater.* **2018**, 28, 1705048.
27. S. Kitagawa, M. Munakata, T. Tanimura, *Inorg. Chem.*,**1992**, 31, 1714.
28. O. M. Yaghi, G. Li, H. Li, *Nature*, **1995**, 378, 703.
29. O. M. Yaghi, H. Li, *J. Am. Chem. Soc*, **1995**, 117, 10401.
30. H. Furukawa, K. E. Cordova, M. O'Keffe, O. M. Yaghi, *Science*, **2013**, 341, 1230444.
31. N. L. Rosi, J. Eckert, M. Eddaoudi, D. T. Vodak, J. Kim, M. O'Keffe, O. M. Yaghi, *Science*, **2003**, 300, 1127.
32. K. –S, Lin, A. K. Adhikari, C. –N. Ku, C. –L. Chiang, H. Kuo, *Int J Hydrogen Energy*, **2012**, 37, 13865.
33. N. –L. Liu, S. Dutta, R. R. Salunkhe, T. Ahamad, S. M. Alshehri, Y. Yamauchi, C. –H. Hou, K. C. –W. Wu, *Sci. Rep*. **2016**, 6, 28847.
34. F. –K. Shieh, S. –C. Wang, S. –Y. Leo, K. C. –W. Wu, *Chem. Eur. J*. **2013**, 19, 11139.
35. S. Gadipelli, T. Zhao, S. A. Shevlin, Z. Guo, *Energy Environ. Sci*., **2016**, 9, 1661.
36. J. Tang, R. R. Salunkhe, H. Zhang, V. Malgras, T. Ahamad, S. M. Alshehri, N. Lobayashi, S. Tominaka, Y. Ide, J. H. Kim, Y. Yamauchi, *Sci. Rep*. **2016**, 6, 30295.
37. M. Hu, J. Reboul, S. Furukawa, N. L. Torad, Q. Ji, P. Srinivasu, K. Ariga, S. Kitagawa, Y. Yamauchi, *J. Am. Chem. Soc*. **2012**, 134, 2864.
38. S. J. Yang, T. Kim, J. H. Im, Y. S. Kim, K. Lee, H. Jung, C. R. Park, *Chem. Mater*. **2012**, 24, 464.